THE JOURNAL OF PHYSICAL CHEMISTRY B

Article

pubs.acs.org/JPCB

Ionic Liquid versus Li^+ Aqueous Solutions: Water Dynamics near Bistriflimide Anions

Chiara H. Giammanco, Patrick L. Kramer, and Michael D. Fayer*

Department of Chemistry, Stanford University, Stanford, California 94305, United States

ABSTRACT: The ultrafast dynamics of concentrated aqueous solutions of the salt lithium bistriflimide and ionic liquid (IL) 1-ethyl-3-methylimidazolium bistriflimide was studied using two-dimensional infrared (2D IR) vibrational echo and polarization-selective IR pump−probe techniques to monitor water's hydroxyl stretch. Two distinct populations of hydroxyl groups, with differing vibrational lifetimes, are detected in solution: those engaged in hydrogen bonding with other water molecules and those engaged in hydrogen bonding with the bistriflimide anion. Water molecules with the same hydrogen bond partner exhibit similar vibrational lifetimes in the two solutions. The reorientation dynamics of the anion-associated waters is also similar in form in the two solutions, showing a restricted wobbling-in-a-cone motion followed by a slower diffusive orientational randomization. However, the wobbling motions are much more angularly restricted in the IL solution. Spectral diffusion dynamics, which tracks the structural fluctuations of water's hydrogen bonds, is very different in the two solutions. Water in the IL solution experiences much faster fluctuations overall and shows a greater extent of motional narrowing, resulting in a larger homogeneously broadened component in the spectral line, compared to those in the aqueous lithium salt. Thus, even when the hydroxyls of water associate with the same anion in solution, the cation identity and extent of ionic ordering (i.e., salt solution vs IL) can play an important role in determining the structural fluctuations experienced by a small hydrogen-bonded solute.

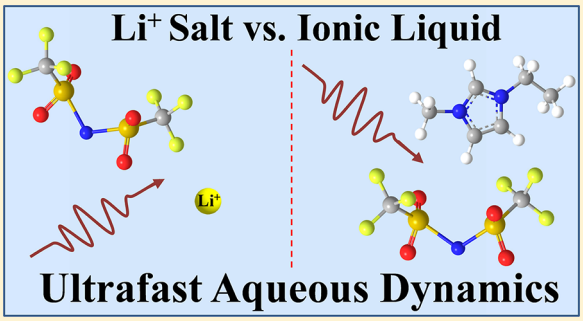

I. INTRODUCTION

Ionic liquids (ILs) are salts that remain liquid below a certain low-temperature threshold, typically set at 100 °C. Additionally, those that remain molten at room temperature are referred to as room-temperature ILs (RTILs). These salts tend to consist of ions with a large degree of asymmetry and flexibility ("floppiness"), leading to a high entropic cost of crystallization.[1,2] The liquid will still try to maintain local charge neutrality leading to charge alternation ordering, but this is not as strict as that found in a crystal because of the high degree of charge delocalization.[2,3]

Recently, ILs have garnered considerable interest for potential industrial applications.[4−6] The aprotic IL materials generally have very low vapor pressure and thus are attractive as "green" solvents that do not suffer evaporative loss into the environment. They can be tuned to be task specific as there are numerous combinations of cations and anions that maintain RTIL behavior and yet have very different chemical properties. ILs can be made to have both polar and apolar regions and thus are attractive for separations as well as allowing reactions that would otherwise be difficult to perform due to the differing solubilities of the reactants. Additionally, the presence of differently sized domains can lead to a mesoscopic ordering in the fluid, which can be exploited for applications.

1-Ethyl-3-methylimidazolium bistriflimide (EmimNTf$_2$) is a popular IL and the subject of extensive study.[7−10] It is both air- and water-stable and is not very viscous, which makes it easy to work with. Even more attractive, it has a large electrochemical window and good thermal stability, leading to proposals for battery applications.[11−15] Recently, it has also been the focus of carbon capture efforts as it will preferentially dissolve carbon dioxide compared to other flue gases.[16−18]

Many of these ILs are hygroscopic and so understanding how their properties change when they interact with water becomes important because water is frequently present. A good deal of work has been done to understand the dynamics of aqueous salt solutions.[19−32] Recent investigations of ILs with dissolved water have focused on the ultrafast reorientation and structural rearrangement dynamics of water at low concentrations using ultrafast infrared (IR) spectroscopy.[33,34] Nuclear magnetic resonance techniques have yielded complementary information on the translational motions of dissolved water in ILs.[35,36] Water motions are generally found to occur much more rapidly than the structural rearrangements and translational motions of the cations and anions. Fast translational and rotational motions are common for small, neutral tracer molecules in IL solutions, with evidence from both experiments and molecular dynamics (MD) simulations.[37−39] Additional MD investigations have focused on the local interactions of dissolved water.[40−42] At higher water concentrations, water hydrogen bonds are found to fluidize the IL. Similar effects have been noted for hydrogen bonds between cations and anions.[43]

Received: July 16, 2016
Revised: August 18, 2016
Published: August 31, 2016

DOI: 10.1021/acs.jpcb.6b07145
J. Phys. Chem. B 2016, 120, 9997−10009

Because of their close structural relationship, it is of considerable interest to compare the structural dynamics of an ordinary (high-melting-point) salt to that of an IL using the same techniques and metrics. However, to compare liquid-phase dynamics, the ordinary salt must be dissolved. Direct comparison then demands not only an analogous IL but also one that can be studied at similar water concentrations.

Whereas $EmimNTf_2$ is a RTIL, its counterpart lithium bistriflimide ($LiNTf_2$) is an ordinary salt that is crystalline at room temperature. Aqueous $LiNTf_2$ itself has been investigated for battery applications[44] and has a remarkable solubility in water. The salt has also generated interest in its use as the basis for solvate ILs, in which lithium cations are coordinated to molecules such as tetraglyme.[45,46] In IL solutions, the addition of lithium cations has been shown to lead to changes in the structure of the liquid and the arrangement of the bistriflimide about the lithium cation.[47−52] In aqueous solutions, the lithium ion typically has four coordinating waters in the first solvation shell, but it may have up to six coordinating waters.[53] For the concentrations studied here, lithium cations will be under-coordinated by water and be forced to interact significantly with the other ions in solution. Thus, the structuring of water about the ions in the lithium salt solutions can also be different from that in the IL, reflecting a corresponding change in the structure. However, the cation does not always influence the dynamics of water molecules hydrogen-bonded to anions.[54−58] Both $EmimNTf_2$ and $LiNTf_2$ aqueous systems are of interest in their own right and also in comparison with each other to see whether the intriguing properties of ILs extend to water mixtures or whether they behave as any other salt once dissolved.

II. EXPERIMENTAL METHODS

$EmimNTf_2$ was purchased from IoLiTec, dried under vacuum while heating at 60 °C, and stored in a nitrogen atmosphere glovebox. Before use, some IL was syringe-filtered through an Anotop 0.02 μm filter to remove any particles and removed from the glovebox. A solution of 5 mole % HOD (singly deuterated water) in H_2O was added to the IL in approximately equal volume. The vial was shaken to form an emulsion and sonicated for 5 min. The mixture was then left to settle and phase-separate into an upper water-rich layer and a lower water-saturated IL layer. The water content of the lower layer was determined by Karl Fischer titration to be 0.66 waters per $EmimNTf_2$ ion pair.

The $LiNTf_2$ salt solutions were prepared by weight with 5% HOD in H_2O to achieve the target concentration. The solution was then sonicated until all of the salt had been dissolved. This necessitated sonication for up to 45 min, and in the process, the vial and its contents became heated. While this facilitated the solvation of the salt, the contents would sometimes crystallize out when the vial returned to room temperature. Progressively greater water concentrations were targeted until the liquid solution was just at the saturation point.

The solutions were sandwiched between 3 mm CaF_2 windows separated by Teflon spacers. The spacer thickness was 56 μm for the $LiNTf_2$ solution and 150 μm for the $EmimNTf_2$ solution. Absorption spectra were acquired using a Thermo Scientific Nicolet 6700 Fourier transform infrared (FTIR) spectrometer. The spectrum of a sample (IL or salt solution) prepared with pure H_2O was also recorded under identical conditions and was used to subtract the background.

The experiments (two-dimensional (2D) IR and IR pump−probe) were performed using an experimental setup and techniques that have been described in great detail previously.[59,60] Briefly, either three (2D IR) or two (pump−probe) polarized, precision-delayed, ultrashort (~60 fs full width at half-maximum (FWHM)), broadband (~240 cm^{-1} FWHM), IR pulses are crossed in the sample and produce a third-order nonlinear signal, which is heterodyne-detected, either with a dedicated local oscillator pulse that does not traverse the sample (2D IR) or by the second pulse (pump−probe). This signal is then frequency-resolved using a spectrograph and detected with a 32-element mercury−cadmium−telluride array detector. The IR pulses, at a wavelength of about 4 μm, were generated using difference frequency generation between signal and idler frequencies in a silver gallium sulfide crystal. A regeneratively amplified Ti:sapphire laser system operating at 1 kHz pumped a two-pass optical parametric amplifier with a β barium borate crystal, providing signal (~1.3 μm) and idler (~2.0 μm) pulses.

III. RESULTS AND DISCUSSION

The key to this study was achieving a water-to-ion pair ratio that is comparable for the two salts. This was challenging because $EmimNTf_2$ becomes saturated with water and phase-separates at concentrations of 1.5 ion pairs per water (or 0.7 waters per ion pair). Potentially, the solubility would increase with temperature, but this route was not pursued. Thus, the challenge was to obtain the same ratio in the $LiNTf_2$ solutions. The lowest water content that could be achieved was 0.4 ion pairs per water (or 2.5 waters per ion pair). Again, if a higher temperature is employed, the solubility increases significantly. However, even though the water content in the two solutions was not identical, the results obtained were sufficiently different to be noteworthy, with the opposite trend than expected given the extra water in the lithium salt solution.

III.A. Linear Absorption Spectra. The OD stretch of the HOD molecule is essentially a local mode that reports directly on its hydrogen-bonding environment.[61,62] In bulk water, the OD stretch gives rise to a broad inhomogeneous line shape due to the variety of hydrogen-bonding structural motifs present. Stronger hydrogen bonds cause a vibration to appear on the redder side of the line, and weaker bonds correspond to a blue shift. Typically, the addition of salts results in a blue shift (and broadening) in the overall line shape due to the addition of a population of salt-associated waters, which are more weakly hydrogen-bonded than water molecules hydrogen-bonded to other water molecules.[19,20] When dilute water is present in an IL, such that the water molecules are well separated, the absorption line shape narrows and shifts considerably to the blue.[33,34,63] As the water concentration is increased, a greater number of hydroxyls will associate with other water molecules and form a second population. An example of this sort of progression in aqueous salt solutions can be found in the literature.[64]

The linear absorption spectra of the two mixtures are distinctly different. Figure 1 displays these spectra with the background signal subtracted and normalized to the peak of the OD stretch absorption. The peaks at 2645 cm^{-1} in the $EmimNTf_2$ solution and at 2635 cm^{-1} in the $LiNTf_2$ solution correspond to the hydroxyls that are anion-associated. This can be easily demonstrated for the water in ILs by comparison to the spectra of more dilute samples of water in $EmimNTf_2$, in which all water molecules are isolated from each other.[34] As

DOI: 10.1021/acs.jpcb.6b07145
J. Phys. Chem. B 2016, 120, 9997−10009

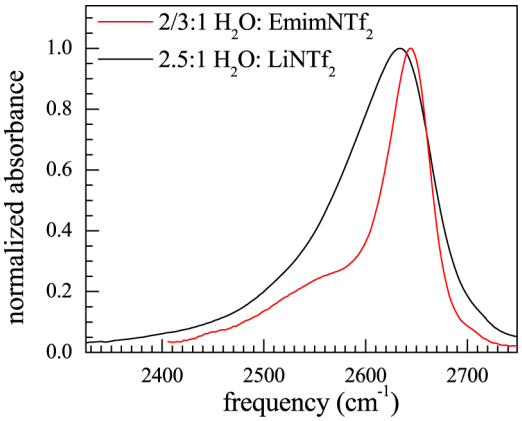

Figure 1. Background-subtracted and normalized absorption spectra of the aqueous solutions of $EmimNTf_2$ (red) and $LiNTf_2$ (black). Note that the two populations (salt-associated and water-associated hydroxyls) are more distinguishable in $EmimNTf_2$. With lithium rather than the imidazolium as the cation, the spectra of the two populations overlap substantially; the asymmetry of the band indicates two populations. Both the anion and water-associated hydroxyls experience a wider range of local environments.

more water is added, the peak to the red develops, centered at ~2570 cm^{-1} for the 2/3:1 water/$EmimNTf_2$ sample shown in red in Figure 1. The lithium cation solution does not show this distinct feature, although this could be partially due to the water-anion spectral differences (being broader and farther red than its IL counterpart) rather than an alteration of the water-associated spectrum. Although more water is present in the 2.5:1 water/$LiNTf_2$ solution than that in the solution of $EmimNTf_2$, this concentration can be compared to that in other IL−water spectra, where the addition of water causes a growth of a distinct water-associated peak.[27,63] Instead of a well-separated band for the water-associated hydroxyls, the $LiNTf_2$ solution presents a clearly asymmetric but not bimodal line shape. Rather than well-defined environments that produce characteristic shifts for the two types of hydroxyls, the Li salt solution provides more varied environments, leading to a broader absorption band. There likely exists a broad continuum of environments for both populations, making them difficult to distinguish based only on the linear absorption profile.

III.B. Vibrational Lifetime. The time constant(s) for vibrational relaxation can be measured with polarization-selective pump−probe experiments. The vibrational lifetime quantifies how long it takes an oscillator to dissipate energy into the bath. The lifetime depends on the immediate surroundings of the oscillator, in particular, the exact energies of low-frequency vibrational modes and coupling strengths to the oscillator.[65] If there are different populations arising from different local structures, as has been inferred from the absorption spectra, the populations typically give rise to noticeably different vibrational lifetimes. These lifetimes can be obtained by resolving the probe polarization following the sample into parallel and perpendicular relative to that of the pump, to give signals $S_{\parallel}(t)$ and $S_{\perp}(t)$, respectively. For this experiment, the pump pulse is polarized at 45°, whereas the probe is fixed at horizontal (0°) before the sample. The pump−probe signals can be expressed in terms of population relaxation, $P(t)$, and the orientational relaxation correlation function, $C_2(t)$:

$$S_{\parallel} = P(t)[1 + 0.8C_2(t)] \quad (1)$$

$$S_{\perp} = P(t)[1 - 0.4C_2(t)] \quad (2)$$

The orientational contribution is $C_2(t) = \langle P_2(\hat{\mu}(t)\cdot\hat{\mu}(0))\rangle$, the second-order Legendre polynomial orientational correlation function of the vibrational transition dipole direction. From these signals, the arbitrarily scaled population relaxation factor can be obtained:

$$P(t) = S_{\parallel}(t) + 2S_{\perp}(t) \quad (3)$$

During the course of the experiment, vibrational relaxation results in a small amount of heat deposition into the excited hydroxyls' surroundings. The transient temperature increase, referred to either as heating or as a "hot ground state", affects the population relaxation signal by producing a long time offset from zero. This heating signal is removed using a well-documented procedure.[66,67]

The population decays for water in the $LiNTf_2$ solution, from slightly red of center to the very blue side of the band, are shown in Figure 2. The inset shows the curves at a short time.

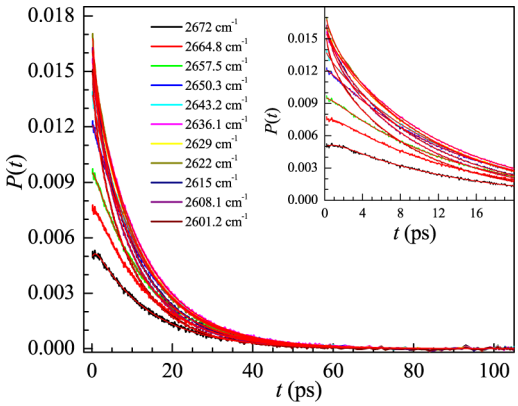

Figure 2. Population relaxation curves for the OD of the HOD stretch in 2.5:1 water/$LiNTf_2$ at wavelengths across the band are shown (colored by frequency, in cm^{-1}), along with global triexponential fits (red). The inset displays the short-time portion of the curves. The very short time component corresponds to fast spectral diffusion, resulting from a non-Condon effect whereby the red side is overpumped and population moves from the red side of the line to the blue. The other two decay times arise from the two populations: water-associated and anion-associated hydroxyls.

Wavelengths farther to the red are not straightforward to analyze due to overlap with the 1−2 transition. The wavelength-dependent decays are fit to triexponential functions with the time constants shared among the curves, but the amplitudes freely varied. At very early times, there is a very fast decay that shows up with a negative amplitude (a growing exponential) on the blue side of the band and zero amplitude at the center that transitions to positive (a decaying exponential) on the red side. The buildup can be clearly seen for some of the curves in the inset. This is consistent with the observation of a non-Condon effect, that is, the transition dipole moment varies across the band and is larger at redder frequencies.[68] The red side becomes slightly overpumped (more excited-state population than the number density) with respect to the blue side. This overpopulation on the red side is transferred toward the equilibrium population distribution by spectral diffusion, resulting in an extra decay on the overpumped red side and a growth on the underpumped blue side.[34] This population movement occurs with the fastest spectral diffusion time

DOI: 10.1021/acs.jpcb.6b07145
J. Phys. Chem. B 2016, 120, 9997−10009

(measured independently; see Section III.D). Components of spectral diffusion with time scales similar to or longer than the vibrational lifetimes typically are not detectable in the population decays. The remaining two exponential decays correspond to other processes, which cause the population to decay. The time constants for the two decays are constant across all wavelengths in the global fit, and their amplitudes vary systematically across the band. This is clear evidence for two separate populations of hydroxyls, which have vibrations that relax on different time scales because these occur in distinct environments with differing bath modes and/or couplings available.[65]

The fits across the band of HOD in 2.5:1 water/$LiNTf_2$ (see Figure 2) correspond to spectral diffusion occurring on a time scale of 0.8 ± 0.1 ps and vibrational lifetimes of T_1^w = 7.0 ± 0.5 ps and T_1^s = 13.4 ± 0.2 ps. The amplitudes corresponding to these lifetimes vary across the band. The amplitude of each component is a direct measure of the relative number of oscillators in that population (if the transition dipole moment magnitudes at a particular wavelength are approximately equal). Thus, as one progresses across the band, there is a transition from the population with the longer lifetime to the blue to a population with the shorter lifetime to the red. The long-lived population, in analogy with other salt solutions and in agreement with the FTIR spectra, is assigned to the salt-associated hydroxyls and the shorter lifetime to the water-associated hydroxyls.

The same analysis can then be performed for the $EmimNTf_2$ solutions. As the peaks are so well defined, it is also possible to fit the FTIR spectrum to obtain the estimates of the expected fractions. Note that peak fitting linear spectra are nontrivial − they generally have Voigt line shapes that are difficult to fit when peaks overlap − but approximate values are easily obtainable. When the populations are fixed to these fractions, the same values (within error) are obtained for the vibrational lifetimes from the population relaxation fits as when the amplitudes are freely left to float.

The population decay data and triexponential global fit results for water in $EmimNTf_2$ are shown in Figure 3, with a wavelength range similar to that for water in $LiNTf_2$. The inset shows the short-time behavior. Again, the fast component is caused by spectral diffusion. The buildup can be seen for some of the curves taken at blue wavelengths. The fits across the band of HOD in 1.5:1 water/$EmimNTf_2$ reveal a component of spectral diffusion occurring on a time scale of 0.7 ± 0.1 ps, as well as vibrational lifetimes of T_1^w = 8 ± 1 ps and T_1^s = 17 ± 2 ps. The vibrational lifetimes for both solutions are collected in Table 1. Note that the values for water in $EmimNTf_2$ are quite similar to the two relaxation time scales in the $LiNTf_2$ solutions, albeit a bit slower. The water in both solutions is clearly experiencing a non-Condon effect, seen in the similar short-time decay. This is a good indicator of the hydroxyls donating moderate-strength hydrogen bonds, akin to the hydrogen bond network of pure water.[34,68,69]

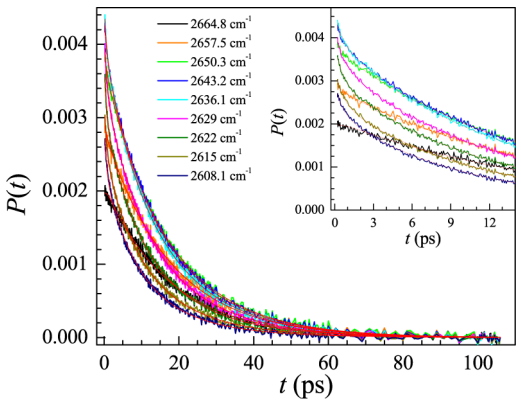

Figure 3. Population relaxation curves for the OD of the HOD stretch in 2/3:1 water/$EmimNTf_2$ are shown (colored by frequency, in cm^{-1}), along with a triexponential global fit (red). The inset displays the short-time portion of the curves. The very short time component corresponds to fast spectral diffusion, resulting from a non-Condon effect whereby the red side is overpumped and the population moves from the red side of the line to the blue. The other two decay times arise from the two populations: water-associated and anion-associated hydroxyls.

III.C. Reorientation. The reorientation of the HOD molecules is directly accessed from the measured parallel and perpendicular signals, described in eqs 1 and 2 above. Orientational relaxation parameters are obtained from the pump−probe data by calculating the polarization anisotropy, $r(t)$, from the difference between the parallel and perpendicular signals:

$$r(t) = \frac{S_{\parallel}(t) - S_{\perp}(t)}{S_{\parallel}(t) + 2S_{\perp}(t)} \tag{4}$$

In the case when only a single population of oscillators contributes to the pump−probe decays, the anisotropy is directly proportional to the second Legendre polynomial orientational correlation function: $r(t) = 0.4C_2(t)$, as obtained from eqs 1 and 2. Although we expect that two populations with different lifetimes will contribute to the pump−probe signals for the water in $LiNTf_2$ and $EmimNTf_2$, the anisotropy is still the preferred parameter by which to visualize the overall orientational relaxation.

The HOD anisotropy decays for wavelengths from slightly red of center to the blue edges of the bands are shown for water in $LiNTf_2$ in Figure 4 and for water in $EmimNTf_2$ in Figure 5. The shortest time delay shown is 200 fs; at shorter times, a nonresonant signal that tracks the pulse durations obscures the OD stretch resonant signal. From Figures 4 and 5, it can be seen that the measured anisotropy decays do not extrapolate to 0.4 at t = 0 as in the ideal case above. The difference between 0.4 and the extrapolate t = 0 value is caused by an ultrafast inertial reorientation component that occurs on a time scale of <100 fs.[70] Although we cannot assign a time constant to this ultrafast inertial motion, its angular range is obtained quantitatively as discussed below.

Within experimental error, the anisotropy decay of HOD in pure water is a single exponential with a time constant of 2.6 ps.[28,67] If there are two populations in solution, they may have different reorientation time scales than those in bulk water and from each other. As the populations also have different lifetimes, we use a function weighted by the lifetimes to fit the measured anisotropy:[71]

$$r(t) = r_0\left[\frac{A\, e^{-t/T_1^w} R_w(t; \tau_{or}^w) + (1 - A)\, e^{-t/T_1^s} R_s(t; B, t_1, t_2)}{A\, e^{-t/T_1^w} + (1 - A)\, e^{-t/T_1^s}}\right] \tag{5}$$

where A is the fraction of the water-associated hydroxyl population with normalized orientation function R_w; $(1 - A)$ is the fraction and R_s is the orientation function of the salt-associated population, and r_0 is an overall normalization factor.

DOI: 10.1021/acs.jpcb.6b07145
J. Phys. Chem. B 2016, 120, 9997−10009

Table 1. Vibrational Lifetimes of the Two Populations and Reorientation Time Constants for Diffusion and Wobbling from Two-Component Fits to the Pump−Probe Anisotropy for Water in Bistriflimide Solutions

sample	T_1^w (ps)	T_1^s (ps)	τ_{or}^w (ps)	τ_{wob}^s (ps)	τ_{or}^s (ps)
2.5:1 water/$LiNTf_2$	7.0 ± 0.5	13.4 ± 0.2	6.9 ± 0.1	1.8 ± 0.1	28 ± 1
2/3:1 water/$EmimNTf_2$	8 ± 1	17 ± 2	10.5 ± 0.5	2.2 ± 0.2	21 ± 2

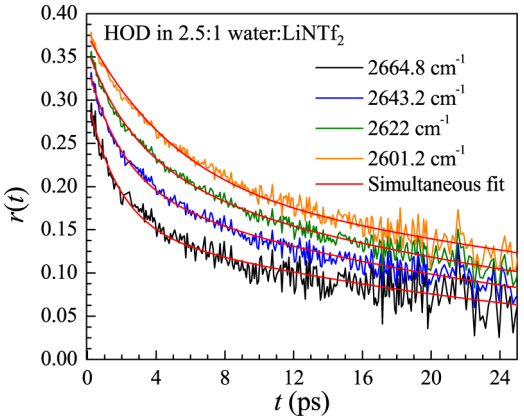

Figure 4. Pump−probe anisotropy orientational relaxation curves for selected wavelengths across the band for HOD in 2.5:1 water/$LiNTf_2$ are shown (colored by frequency), along with fits using eq 5 (red). There are two populations, each with its own vibrational relaxation and reorientation times. Additionally, the anion-associated population undergoes a restricted wobbling motion on a fast time scale.

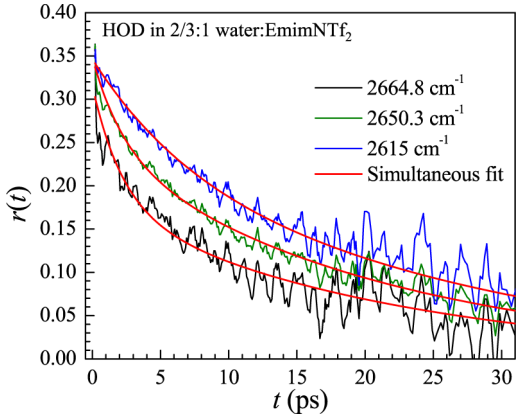

Figure 5. Pump−probe anisotropy orientational relaxation curves for selected wavelengths across the band for HOD in 2/3:1 water/$EmimNTf_2$ are shown (colored by frequency), along with fits using eq 5 (red). There are two populations, each with its own vibrational relaxation and reorientation times, including a wobbling motion for the anion-bound hydroxyls.

This normalization factor accounts for the anisotropy starting value not being 0.4 because of the inertial component of the orientational relaxation. We assume that both populations undergo approximately the same range of inertial motion. It is important to note that although the contributions of both water populations to the individual parallel and perpendicular pump−probe signals are additive, the same does not hold for the anisotropy in eq 5. When the vibrational lifetimes are different, $r(t)$ is not free of population decay influence and the function can exhibit a nonmonotonic behavior.[71] Reorientation and population decay must be fit simultaneously in eq 5, but as the vibrational lifetimes are known, only the orientational parameters are free in the fit.

The orientational correlation is a function of the orientation time, τ_{or}, for each population. For the water-associated population, we employ a single exponential decay corresponding to orientational diffusion by either infinitesimal steps or discrete angular jumps.[72] Thus, $R_w(t) = \exp(-t/\tau_{or}^w)$ is a straightforward fitting function for the water-associated population's reorientation component. For the salt-associated population, there is a constrained rotational diffusion process, which causes the orientational correlation function to decay to an offset before complete orientational diffusion can take place. This constrained motion is referred to as "wobbling", and the wobbling-in-a-cone model is used to interpret the data.[73,74] The orientation function for fitting is given by

$$R_s(t, B, t_1, t_2) = B \exp(-t/t_1) + (1 - B) \exp(-t/t_2) \quad (6)$$

where B is the fraction of the amplitude due to the faster wobbling motion and t_1 is its associated time constant, whereas the longer time scale for complete diffusive randomization is t_2. Equation 6 is in a form convenient for performing the fit to the data using eq 5, but the physical interpretation of the function depends on the model.

Once the anisotropy curves are fit with eqs 5 and 6, a wobbling-in-a-cone analysis[73,75] can be performed to quantitatively characterize both the restricted orientational motions and final diffusive randomization.[34,70,76,77] The restricted wobbling motion is modeled as free diffusion within a cone of a certain half-angle with hard walls. For the systems examined here, there are two cones overall: an initial fast inertial motion, termed the inertial cone, and a wobbling cone. The two restricted reorientation processes are taken to be independent of each other, so their correlation functions are multiplicative. A wobbling period is modeled by an orientational correlation function that decays as a single exponential toward a plateau given by the square of a generalized order parameter:

$$C_2^{wob}(t) = (1 - S^2) \exp(-t/\tau_{wob}) + S^2 \quad (7)$$

The order parameter, S, determined from the data, gives model-independent information on the confining potential, and, within the hard cone model, is straightforward to relate to the cone half-angle, θ_0:[73]

$$S = \frac{1}{2} \cos(\theta_0)(1 + \cos(\theta_0)) \quad (8)$$

r_0 is given by 0.4 times the squared order parameter for the inertial cone. The decay due to the inertial motion (first term in eq 7) has reached zero within the pulse duration.

For the salt-associated population, the restricted diffusive motions are followed by a statistically independent free diffusion, which leads to total randomization, which is incorporated as a multiplicative factor to eq 7 of $\exp(-t/\tau_{or})$.[73] Thus, the complete salt-associated water orientational correlation function is

DOI: 10.1021/acs.jpcb.6b07145
J. Phys. Chem. B 2016, 120, 9997−10009

$$R_s(t; \tau^s_{or}, \tau^s_{wob}, S^2) = (1 - S^2)\exp(-t(1/\tau^s_{wob} + 1/\tau^s_{or})) + S^2\exp(-t/\tau^s_{or}) \quad (9)$$

A comparison to eq 6 allows the fit parameters to be rearranged to yield τ^s_{or}, τ^s_{wob}, and S^2.

Fitting the anisotropy curves for the $LiNTf_2$ solution to eq 5, while holding the lifetimes and fractions fixed to those found from the population decays in Section III.B, yields good fits across the band as shown in Figure 4. The orientational relaxation time constants were fixed in the global fit across all displayed wavelengths, whereas the amplitudes for the wobbling reorientation function in eq 6 were allowed to vary. The reorientation time for the water-associated population was determined to be $\tau^w_{or} = 6.9 \pm 0.1$ ps, that of the NTf_2-associated population was determined to be $\tau^s_{or} = 28 \pm 1$ ps, and the wobbling time was determined to be $\tau^s_{wob} = 1.8 \pm 0.1$ ps. Note that the inertial drop is greater on the blue side of the band than on the red side, consistent with blue side hydroxyls engaging in weaker hydrogen bonds with a softer angular potential.[70]

A similar fitting procedure is employed for the anisotropy curves of the $EmimNTf_2$ solution, again holding the lifetimes and fractions fixed to those found in Section III.B. This gives decent fits across the band, displayed in Figure 5, although the curves are much noisier than those of the lithium salt solution. There are fewer water molecules per unit volume due to both the concentration difference and the fact that the $Emim^+$ cation takes up more space than the lithium cation, leading to a lower signal. However, the reduced number of water molecules was somewhat compensated for by making the IL sample 3 times thicker (150 vs 56 μm path length) than the lithium salt sample but at the expense of increased background absorption. In the IL sample, there is less wavelength variation. The reorientation time for the water-associated population is $\tau^w_{or} = 10.5 \pm 0.5$ ps and that of the NTf_2-associated population is $\tau^s_{or} = 21 \pm 2$ ps. The wobbling time was found to be $\tau^s_{wob} = 2.2 \pm 0.2$ ps.

The reorientation time constants for waters in the $LiNTf_2$ and $EmimNTf_2$ systems are collected in Table 1. The two systems are fairly similar in the reorientation time scales. The water-associated hydroxyls reorient faster in the lithium solution: 6.9 versus 10.5 ps in the IL. Both values are several times slower than the reorientation time of HOD in bulk water (2.6 ps), which has an uninterrupted hydrogen bond network. Despite the fact that $LiNTf_2$ is solvated in liquid water, there does not appear to exist any significant population of water molecules in a bulklike environment at this very high salt concentration. The reorientation of water molecules has been shown to occur in a concerted manner via a jump reorientation model.[31,72,78] In bulk water, jump reorientation involves the first and second "solvation shells" about a particular water molecule. In the concentrated IL and lithium salt solutions, there are a very limited number of water molecules available to participate in jump reorientation. It may be that the waters cannot reorient until the ions permit their neighbors to move.

The presence of the much larger and more slowly diffusing imidazolium cation may be sufficient to cause the slowing of the complete orientational relaxation seen in the IL solution's water-associated hydroxyl population. Opportunities to reorient and form a new hydrogen bond are even more limited for these molecules as compared to those in $LiNTf_2$ solution and bulk water. However, this does not explain the trend in the anion-associated population. The anion-associated hydroxyls experience a slightly slower wobbling in $EmimNTf_2$ (although it is nearly the same as the $LiNTf_2$ solution wobbling time within error), but their complete reorientation occurs with a 21 ps time constant rather than the slower 28 ps of $LiNTf_2$. Looking at the linear spectra (see Figure 1), we see that on average the NTf_2-associated population in the IL is more blue-shifted than its lithium solution analogue. The blue shift suggests that the hydrogen bonds to anions are generally weaker in the IL solution, which may enable the faster reorientation. However, as a whole, the corresponding populations of water in the two solutions reorient with very similar time constants (see Table 1).

The results of the wobbling analysis for the anion-associated water molecules are shown in Figure 6. Panel A shows the inertial cone half-angle across the absorption band for the two solutions. Note that both solutions have anion-associated hydroxyls, which experience roughly the same inertial motions across the band. The water-associated population was successfully fit with an identical inertial cone angle as the anion-associated population, showing that this extremely local

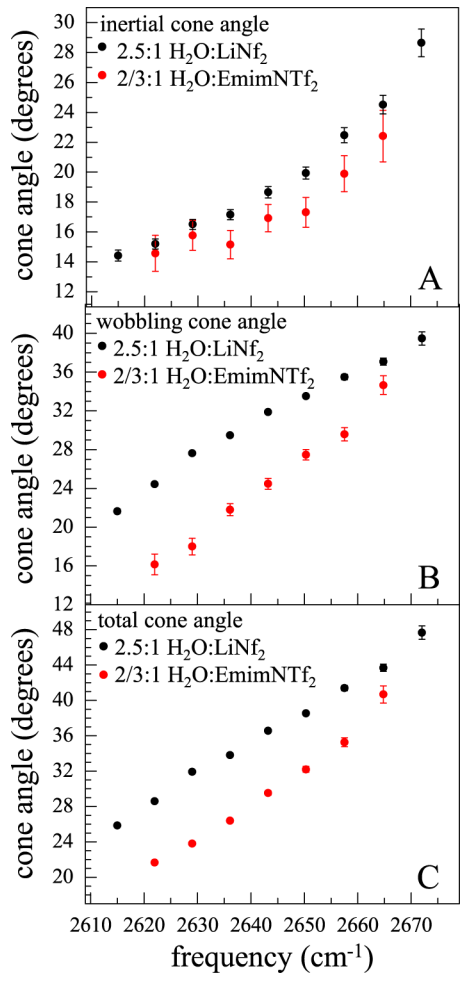

Figure 6. Results of the wobbling-in-a-cone analysis performed on the anisotropy data for the anion-associated water populations in 2.5:1 water/$LiNTf_2$ (black) and 2/3:1 water/$EmimNTf_2$ (red). Panel A shows the inertial cone half-angle across the absorption band for the two solutions. The wobbling cone is in Panel B. Panel C displays the total cone resulting from both restricted reorientation processes taken together. Error bars (in some cases, contained within the symbols) are the propagated standard error of the fit.

DOI: 10.1021/acs.jpcb.6b07145
J. Phys. Chem. B 2016, 120, 9997−10009

motion about an intact hydrogen bond is largely invariant to the H-bond accepter. The wobbling cone wavelength dependence is displayed in Panel B. The wobbling motions are not the same for the two solutions. The IL solution, which has less water, has more restriction of the wobbling motion, resulting in tighter cone angles. Despite the fact that these motions are so restricted, they occur with similar time constants, as noted above. Panel C displays the total cone angle, which is the total angular range sampled by both restricted reorientation processes taken together. It is defined by an order parameter that is the product of the two individual wobbling order parameters. The major contribution is from the (larger) wobbling cone, and so the total cone in C has the same trend as seen in B.

The results of the wobbling analysis are particularly striking when one considers that only the anion-associated population is being examined. The effects of the water-associated hydroxyls have been removed. Each of the contributing hydroxyls in the two solutions is hydrogen-bonded directly to a bistriflimide anion. But clearly the wobbling motion is not solely determined by the anion. The structure around the anion in the IL solution has a confining effect, which further restricts the extent of wobbling. Water in this system is thus sensitive to longer-range structural details of the IL.

Further insight into the constraints on anion-associated hydroxyl rotation can be gained by a comparison with pump–probe anisotropy experiments performed on isolated HOD molecules in $EmimNTf_2$, at a ratio of 1 water per 20 ion pairs.[34] In this case, all water molecules are hydrogen-bonded to anions; there is no water-associated hydroxyl population.[63] The wobbling cone angles across the band (Figure 6B) are extremely similar for both concentrations. However, both the time constants, a wobbling time of about 5 ps and diffusion time of 25 ps, are longer for the lower-water-concentration IL. This is particularly noticeable for the wobbling period, which is over a factor of 2 slower. The existence of small pockets of multiple water molecules (which necessarily include the water-associated hydroxyls visible in the linear absorption; Figure 1) does not noticeably change the range of constraints experienced by anion-bonded waters on shorter time scales, but it apparently does affect the rate at which the constraints are released to allow more orientational sampling on both short and long time scales. The water pockets could be thought of as "lubricating" the native IL structure to allow somewhat faster ion fluctuations and therefore hydroxyl motions; this is consistent with the large drop in bulk IL viscosity that accompanies water addition.[79] The wobbling time scale for water in the $LiNTf_2$ solution is similar to that for the saturated water/$EmimNTf_2$ solution; in both cases, the hydroxyl wobbling around an NTf_2 H-bond partner has been accelerated by the presence of other water molecules in the medium.

III.D. Spectral Diffusion. The normalized frequency–frequency correlation function (FFCF) is the joint probability that a vibrational oscillator with a particular frequency at $t = 0$ will still have the same frequency at a later time t, averaged over all initial frequencies. Structural fluctuations altering the OD stretch frequency of HOD in the two solutions contribute to the decay of the FFCF: as the structure fluctuates, the vibration probed is able to sample a greater portion of its vibrational inhomogeneously broadened absorption line. This process is known as spectral diffusion and can be measured using the 2D IR vibrational echo technique and quantified by the center line slope (CLS) method performed on the resulting 2D spectra.

A 2D IR experiment results in 2D correlation spectra at a series of waiting times between the pump interactions (pulses 1 and 2) that label the initial frequencies and the probe interactions (pulse 3 and signal emission) that read out the final frequency of a resonant oscillator. The final oscillation frequency, ω_3, is plotted against the initial oscillation frequency, ω_1. Here, the numbers 1 and 3 refer to the first and third time periods (interpulse delays) in the 2D IR pulse sequence, with the second time period being the waiting time, T_w. A representative 2D IR spectrum is shown in Figure 7 for

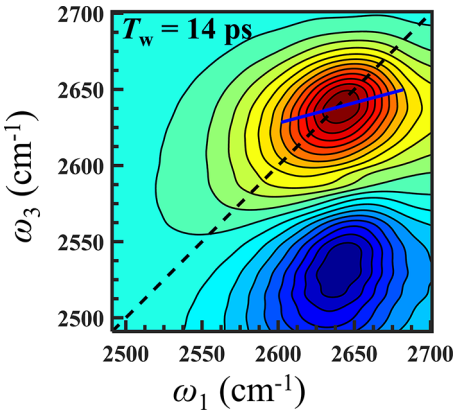

Figure 7. Representative 2D IR spectrum of the OD stretch of HOD in water (5% HOD) in the 2.5:1 water/$LiNTf_2$ solution, at a waiting time of T_w = 14 ps. The diagonal is shown as a black dotted line. The positive-going band on the diagonal is the 0–1 transition, whereas the negative-going band is the 1–2 transition, which is shifted to lower frequency along ω_3 by the vibrational anharmonicity. The solid blue line is the center line, yielding the CLS.

HOD in the $LiNTf_2$ solution at a waiting time of 14 ps. There are two bands corresponding to the OD stretch of HOD in this spectrum. The positive-going band on the diagonal is the 0–1 transition, whereas the negative-going band below it is the 1–2 transition. The 1–2 transition is shifted along ω_3 to the red by the vibrational anharmonicity. The 1–2 band shape generally reports the same information as the 0–1 band shape, so only the 0–1 transition will be analyzed.

The CLS is determined in two steps. First, the slices parallel to ω_3 at a series of ω_1 values are taken around the center of the band. Each of these is a spectrum, and the frequency of the maximum value is determined. These ω_3 peak values are plotted against the ω_1 slice position to generate the center line. The center line (blue line) is shown in Figure 7. A linear fit to the center line gives the slope of this center line, which is defined as the CLS.[80] As the T_w is increased, spectral diffusion causes the shape of the 2D spectrum to change (becomes more round), and the CLS changes. Therefore, the CLS is a function of T_w, (CLS(T_w)). The maximum value of the CLS is 1 and the minimum value, when spectral diffusion is complete, is 0.

The CLS(T_w) is equal to the normalized FFCF.[80,81] The measured spectral diffusion (FFCF decay) is a direct reporter of the structural fluctuation time scales and can be modeled as a sum of exponentials, one for each time scale process. The complete correlation function may be written as

$$C(t) = \langle \delta\omega(t)\delta\omega(0)\rangle = \sum_i \Delta_i^2 \exp(-t/\tau_i) \tag{10}$$

where $\delta\omega(t) = \omega(t) - \langle\omega\rangle$ is the instantaneous frequency fluctuation. Δ_i are the amplitudes and τ_i are the correlation

DOI: 10.1021/acs.jpcb.6b07145
J. Phys. Chem. B 2016, 120, 9997–10009

times of the frequency fluctuations induced by the structural fluctuations of the solution. If a component i is in the motionally narrowed limit, $\Delta_i\tau_i < 1$. Δ_i and τ_i cannot be determined independently. The motionally narrowed contribution to the FFCF is a component of the homogeneous pure dephasing, that is, it contributes to the homogeneous linewidth. The motionally narrowed contribution to the absorption spectrum has a pure dephasing linewidth, given by $\Gamma^* = \Delta^2\tau/\pi = 1/\pi T_2^*$, where T_2^* is the pure dephasing time. The total homogeneous dephasing time that is measured, T_2, also depends on the transition dipole orientational relaxation and vibrational lifetime and is given by

$$\frac{1}{T_2} = \frac{1}{T_2^*} + \frac{1}{2T_1} + \frac{1}{3T_{or}} \tag{11}$$

where T_1 and T_{or} are the vibrational lifetime and orientational relaxation time, respectively. The CLS result, in conjunction with the linear absorption spectrum of the vibrational probe, enables the determination of the homogeneous contribution to the linewidth and the resulting full FFCF to be obtained.[80,81]

Even though there are two populations in both solutions, water- and anion-associated hydroxyls, the spectral diffusion could only be accessed for the anion-associated population. The lower-frequency water-associated hydroxyls do not yield sufficient signal and are complicated by overlap from the 1−2 transition of the anion-associated population. The spectral diffusion (structural fluctuations) of the anion-associated populations, quantified by the CLS technique, is shown in Figure 8. It is evident that the spectral diffusion dynamics in these two solutions are not the same. Part of this, of course, is due to the difference in water concentration. However, as can be clearly seen in Figure 8, the difference is striking and in the opposite direction from that expected: the presence of more water typically will speed up a decay because water's structural fluctuations occur fairly quickly when uninhibited by ions[20,82−84] and additional water will lower the viscosity of a high-concentration salt solution. Yet, the anion-associated water population in $EmimNTf_2$ exhibits faster overall structural relaxation even through the solution contains less water per ion pair.

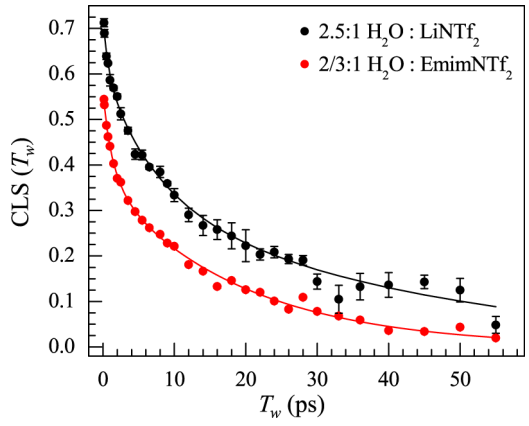

Figure 8. Spectral diffusion, as quantified by the CLS method, for HOD in 2.5:1 water/$LiNTf_2$ (black points) and 2/3:1 water/$EmimNTf_2$ (red points). Each curve is the average of several runs, and the error bars are the standard deviation. The error bars for the red curve are contained inside the data points. The solid curves are triexponential fits to the data.

The spectral diffusion for both solutions can be fit to triexponential decays. The 2.5:1 water/$LiNTf_2$ CLS fits to time constants of 0.8 ± 0.2, 7 ± 2, and 40 ± 10 ps. The 2/3:1 water/$EmimNTf_2$ CLS decays fit to time constants of 0.7 ± 0.2, 1.9 ± 0.5, and 19 ± 2 ps. The time constants are also given in Table 2 for easier comparison. Both have a fast process of spectral diffusion that occurs on the same time scale within error. This could be caused by hydrogen bond length fluctuations that result in a spectral diffusion component of 0.4 ps in bulk water, which has now been slowed down because of the presence of ions. As has been seen previously,[20,29] salt solutions often cause a slowing of this first spectral diffusion time scale, particularly as the concentration is increased. However, after this initial time scale, the two solutions have quite different dynamics. The dynamics of water associated with the anions in the $LiNTf_2$ solution is significantly slower than in the IL solution.

There can be several reasons for why the dynamics differs in the two solutions (Table 2). The IL solution is saturated with water, whereas the regular lithium salt solution is at its lowest water concentration. As shown in the linear absorption spectra (Figure 1), in the IL, the spectral feature of the water-associated population is more distinct from its NTf_2-associated counterpart than that in the $LiNTf_2$ solution. The anion-associated hydroxyls in $EmimNTf_2$ are predominantly isolated from other waters and solvated within the native IL ionic region structure.[34,63] As discussed in Section III.C, for the reorientation dynamics in the saturated IL solution, the presence of water clusters or pools tends to speed up the ion fluctuations around their equilibrium positions, resulting in faster fluctuations of the hydroxyl H-bond interactions and thus the vibrational frequency. Compared to the spectral diffusion dynamics of water at a very low concentration in $EmimNTf_2$, the FFCF decays after the ultrafast 700 fs component are indeed accelerated for the 2/3:1 water/$EmimNTf_2$ solution.[34]

Unlike the case of water in an IL solution, the very high salt concentration in the $LiNTf_2$ aqueous solution results in a severe slowing of anion-bonded hydroxyl fluctuations compared to those in the water in both lower-concentration salt solutions[20] and predominantly dry ILs.[34] At the highest $LiNTf_2$ concentrations, such as that in our 2.5:1 water/$LiNTf_2$ mixture, both the water molecules and ions appear locked in an intermolecular structure distinct from both bulk water or dilute

Table 2. FFCF Parameters for Water in Bistriflimide Solutions

sample	Γ (cm^{-1})[a]	Δ_1 (cm^{-1})	τ_1 (ps)	Δ_2 (cm^{-1})	τ_2 (ps)	Δ_3 (cm^{-1})	τ_3 (ps)
2.5:1 water/$LiNTf_2$	14.0 ± 0.7	12.8 ± 1.0	0.8 ± 0.1	17 ± 3	7 ± 2	20.4 ± 2.6	40 ± 10
2/3:1 water/$EmimNTf_2$	15.7 ± 0.3	5.9 ± 0.3	0.7 ± 0.1	7.2 ± 0.2	1.9 ± 0.5	11.8 ± 0.6	19 ± 2

[a]The homogeneous linewidth, Γ, is the FWHM of the Lorentzian contribution to the total linewidth, whereas the Δ_i's are the standard deviations of the individual Gaussian inhomogeneous contributions. The total inhomogeneous linewidth (standard deviation) is $\sqrt{\Delta_1^2 + \Delta_2^2 + \Delta_3^2}$. The FWHM is 2.355 times the standard deviation. The total line shape is the convolution of the Lorentzian and the total Gaussian contributions.

DOI: 10.1021/acs.jpcb.6b07145
J. Phys. Chem. B 2016, 120, 9997−10009

salt solutions and ILs. None of the water present in the $LiNTf_2$ solution could be assigned as a bulklike component (Section III.C). There are fewer opportunities for fluctuations around the hydroxyl equilibrium positions in this dense aqueous-ionic network, which has a less fluid interior than that of a dry or hydrated IL.

When less water is added to the $EmimNTf_2$ solution, the CLS curve slows, as shown in Figure 9A, approaching the result

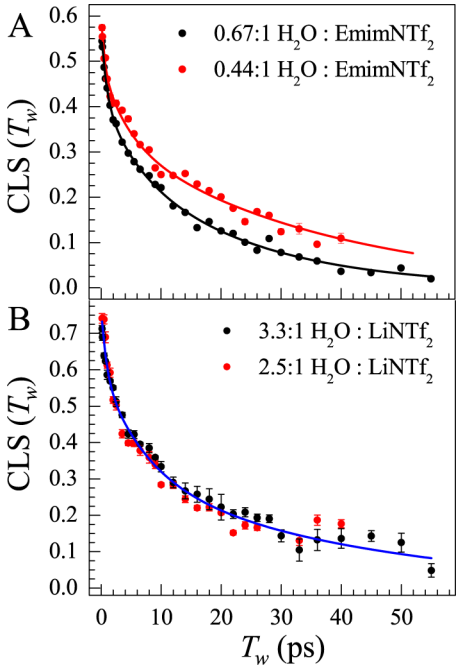

Figure 9. Spectral diffusion, as quantified by the CLS method, for the anion-associated HOD in the hydrated IL and aqueous lithium salt solutions. Panel A shows 0.67:1 (black) and 0.44:1 (red) water/$EmimNTf_2$ solutions. Panel B shows 3.3:1 (black) and 2.5:1 (red) water/$LiNTf_2$ solutions. Lines are added as guides to the eye. The higher water concentrations are shown in black. Reducing the water concentration in the IL slows the spectral diffusion dynamics, whereas the lithium salt solution shows no change in the spectral diffusion within experimental error.

for extremely dilute water in $EmimNTf_2$, in which all hydroxyls are anion-bonded.[34] However, when more water is added to the $LiNTf_2$ solution, a very little change is observed (Figure 8B). Note that these curves are all derived via the CLS method on the anion-associated peak and so only report on changes in the dynamics of this population, as with the results in Figure 8 and Table 2. The top panel shows the effect of slightly lowering the water concentration in the IL. Upon decreasing the waters per ion pair from 0.67 to 0.44, the structural dynamics undergoes a slowing in the longer-time-scale motions. In contrast, the lower panel shows the behavior exhibited in the $LiNTf_2$ solutions. The increase in water concentration from 2.5 waters per ion pair to 3.3 waters causes a very little change in the observed dynamics. Because the concentrations of the two solutions could not be overlapped, it is possible that the solutions exist in different concentration regimes along the same path of states. There might be a threshold for a change in structure above which the concentration has less importance. However, we have already demonstrated that the lithium solution, which has higher water concentration than the IL solution, exhibits slower structural fluctuations. If the dynamics was purely a matter of threshold and concentration, then the IL solutions (with their lower water concentrations) should exhibit slower dynamics when in fact it is faster.

Recently, it has been observed that vibrational probes in ILs may experience reorientation-induced spectral diffusion (RISD).[77,85−87] This effect results from the rotation of the probe that alters its directional interactions with the surroundings and thus the observed frequency. RISD is a contribution to the measured spectral diffusion in addition to the structural fluctuations. The hallmark of RISD is observing different spectral diffusion decays based on the polarizations of the incident beams (e.g., pump interactions perpendicular to the probe result in a faster decay than that when all beams had parallel polarization). If it is present, the goal is to separate the effect of RISD from the spectral diffusion data and to recover the effect of the structural fluctuations alone, given that the rotational contribution is characterized entirely by the independent polarization-selective pump−probe measurements.[85,86] Typically, multiple polarization vibrational echo experiments are executed and fit simultaneously to recover the structural fluctuations, but there is no reason why a single polarization experiment cannot be used to obtain both the structural spectral diffusion (SSD) and the RISD. It has been shown that such fits yield the same numbers, within experimental error, as the simultaneous fits.[77]

For the data sets here, the experiments were performed in a single polarization geometry, in which all of the incoming beams had parallel polarization. As the rotational dynamics was determined from pump−probe experiments, these numbers could be fixed. The RISD function corresponding to a first-order Stark effect model (appropriate for H-bonded hydroxyls)[86,87] was fit to the CLS data. The SSD parameters that the fits yielded were the same within error as those obtained from the direct fits of the decays. Thus, if there is RISD in this system, its effect is minimal. Because RISD was found to have a small effect, no additional polarization configuration data are required to accurately determine the structural fluctuation dynamics.

The complete FFCF including the homogeneous linewidth was calculated using the triexponential fits to the CLS data in conjunction with the linear spectra,[80] and the resulting parameters are given in Table 2. Note that linear spectra were needed to determine the homogeneous component and distinguish it from the first spectral diffusion time-scale amplitude. As these spectra were composed of two populations and yet the spectral diffusion parameters were obtained from the anion-associated hydroxyls only, the bounds of the fit of the FTIR spectra had to be limited to only the contributing wavelengths. The $EmimNTf_2$ solution absorption was fit from 2630 to 2775 cm^{-1} and that of $LiNTf_2$ from 2610 to 2775 cm^{-1} in the FFCF calculation. Because of the concern that both these segments, though primarily anion-associated, may still have small contributions from the water-associated hydroxyls on the red side, the anion-associated spectra from the multiple peak fits of the FTIR spectra (discussed briefly in Section III.A) were used in a second FFCF calculation. The second calculation gave the same numbers, within error, as the FFCF calculation with the bounded, unaltered linear spectra. Because of the overlap of the anion-associated spectrum with the water-associated spectrum, there is some error in the fits, but it is not large. The errors in fitting the spectra are in part reflected in the error bars on Γ and Δ_1 in Table 2.

DOI: 10.1021/acs.jpcb.6b07145
J. Phys. Chem. B 2016, 120, 9997−10009

The anion-associated water in $EmimNTf_2$ has a narrower linewidth (~44 cm^{-1}) than that of the water in $LiNTf_2$ solution (~78 cm^{-1}). Nevertheless, the ion-associated hydroxyl in the IL has a slightly larger homogeneous component of the linewidth. When considered in terms of percentage of the line, the difference is significant: 35% for the IL solution versus 18% for the lithium salt solution. In contrast, the three inhomogeneous contributions to the absorption line are approximately twice as large in magnitude in the lithium cation liquid compared to those in the 1-ethyl-3-methylimidazolium-containing liquid. However, the inhomogeneous contributions, which are sampled by spectral diffusion, represent similar percentages of the total linewidths and thus are independent of the cation identity. This might suggest that the same types of structural variations occur that inhomogeneously broaden the lines, but the coupling strength of the vibration to the structural variations is weaker in the IL solution, producing a smaller inhomogeneous broadening magnitude but the same percentage of the line as that in the lithium salt solution.

IV. CONCLUDING REMARKS

The dynamics of HOD in aqueous solutions of $EmimNTf_2$ and $LiNTf_2$ has been fully characterized at the highest and lowest water concentrations, respectively. Although the same concentration of water could not be attained due to unavoidable solubility limits at room temperature, the concentrations examined were sufficient to draw conclusions about the difference in dynamics that a change in cation (resulting in a drastically altered liquid environment) can cause. The linear spectra for the two solutions are very different, though each can be decomposed into two populations: water-associated hydroxyls and anion-associated hydroxyls. The hydrogen bonding to the anion is somewhat weaker in the IL solution than that in the lithium solution on the basis of the linear spectra, in which the absorption by the OD hydroxyls bound to NTf_2 anions is at higher frequency in the IL than in the lithium salt solution.[88,89] It is noteworthy that the peaks of the ODs associated with water spectra are virtually at the same wavelength. Although there is error because of the difficulty in fitting the total spectra to determine the peaks of the water-associated bands, the values obtained for the IL and the lithium salt solutions are ~2570 and ~2580 cm^{-1}, respectively. This indicates that the ODs hydrogen-bonded to water molecules have similar hydrogen bond strengths. However, both bands are significantly blue-shifted from those of HOD's absorption in bulk H_2O, where the peak position is 2509 cm^{-1}.[56] Therefore, the hydrogen bonds to water in the solutions studied here are significantly weaker than those in bulk water. The weaker hydrogen bonding indicates that the water−water structure cannot obtain the optimal quasitetrahedral arrangement found in bulk water.

Because the ratios of the anion-associated and water-associated hydroxyl populations vary across the absorption spectra, their dynamical contributions to a specific wavelength vary proportionately. This ratio of populations was taken into account when interpreting the vibrational relaxation and reorientation data. The vibrational lifetimes of both populations were measured and were found to be similar in the two solutions. Given that the vibrational relaxation is determined by local interactions, the results indicate that these interactions are comparable in the IL and in lithium salt solutions. The water-associated population relaxes more quickly than the population hydrogen-bonded to the NTf_2 anion. Although the vibrational relaxations in the two solutions are similar, they are not identical. It takes longer for the anion-associated population to relax in $EmimNTf_2$ than in $LiNTf_2$. This is consistent with the hydroxyl making a weaker hydrogen bond with the anion in $EmimNTf_2$ than in $LiNTf_2$, as indicated by the blue shift of the OD hydroxyl absorption in the $EmimNTf_2$ solution compared to that in the $LiNTf_2$ solution.

The reorientation was fit using a two-component model to account for the two populations, and a wobbling motion preceding complete orientational relaxation was found to occur for the anion-associated hydroxyls. In bulk water, orientational relaxation occurs as a single exponential (2.6 ps) with no wobbling component following the ultrafast inertial motion; the water-associated populations here were found to behave likewise, with a single exponential decay. The reorientation dynamics was found to be somewhat, but not greatly, different in the two solutions (see Table 1). The hydroxyls hydrogen-bonded to other water molecules relax more slowly in the IL, but the hydroxyls bound to anions relax more slowly in the lithium solution. However, the differences are only ~30%. The wobbling time constants are almost identical. As revealed by the wobbling-in-a-cone analysis, the local angular restrictions on the wobbling motions are much more confining in the lower-water-content IL than in the lithium salt solution. The structure of the solution is sufficiently different; thus, the dynamics is affected to some extent, even though the water is hydrogen-bonded to the same anion.

The OD hydroxyl spectral diffusion, which reports directly on the structural fluctuations of the liquid, is very different in the two salt solutions. Not only did the $LiNTf_2$ solution experience slower motions, but it also showed an opposite trend to that expected given its higher water concentration. The IL sees structural fluctuations occurring twice as fast as well as a larger homogeneous component, which occurs because of ultrafast motionally narrowed structural fluctuations.

The dynamics shown by the OD hydroxyls is dominated by their hydrogen bonding with the NTf_2 anions. Because the cations are very different, it might be anticipated that the dynamics in the two salt/water solutions would differ. The $LiNTf_2$/water solution has considerably more water in it than that in the $EmimNTf_2$/water solution. Nonetheless, the dynamics reported by the hydroxyls in the lithium salt solution is slower than that in the IL solution despite the expectation that more water leads to faster dynamics. The faster structural fluctuations in the IL solution may arise from the fundamental differences in the nature of the two liquids. The $LiNTf_2$/water solution is only a liquid because of the presence of water. If the water concentration is reduced, $LiNTf_2$ crystallizes. In the liquid, water is intimately involved in the liquid structure. To form a liquid, water must solvate the anions and cations. When the amount of water is in the range of just dissolving the crystalline material, there is little flexibility in the arrangement of the water molecules to give the optimal structure for solvating the ions. Thus, the water is in a structure that inhibits rapid structural rearrangement. Addition of a small amount of water improves the solvation but still leaves a relatively well defined structure that has little change in dynamics (see Figure 9B).

The IL is fundamentally different. It is a liquid without any water. The liquid structure is dominated by the anion−cation interactions, with a tendency to have charge alternation.[2,3] When water is added, it is an interloper in the IL. Water does not have a profound influence on the structure of the liquid,

DOI: 10.1021/acs.jpcb.6b07145
J. Phys. Chem. B 2016, 120, 9997−10009

and phase separation occurs at quite low water content, demonstrating that the IL−water interactions are not particularly favorable. The result is that water may not be as restricted in its structural configurations in the IL as it is in the lithium salt solution. However, water may act to lubricate the motions of the IL, but without imposing severe constraints on the water configurations, leading to faster dynamics. When the water concentration is reduced, the lubricating influence is reduced and the IL−water spectral diffusion dynamics slows (see Figure 9A). The net result is that although the anion that hydrogen-bonds with water is the same in $LiNTf_2$ and $EmimNTf_2$, the role of water in the two liquids is very different; thus it is, in part, responsible for the difference in the dynamics.

AUTHOR INFORMATION

Corresponding Author

*E-mail: fayer@stanford.edu. Phone: (650) 723-4446.

Notes

The authors declare no competing financial interest.

ACKNOWLEDGMENTS

This work was funded by the Division of Chemical Sciences, Geosciences, and Biosciences, Office of Basic Energy Sciences of the U.S. Department of Energy through grant # DE-FG03-84ER13251.

REFERENCES

(1) Castner, E. W.; Margulis, C. J.; Maroncelli, M.; Wishart, J. F. Ionic Liquids: Structure and Photochemical Reactions. *Annu. Rev. Phys. Chem.* **2011**, *62*, 85−105.

(2) Hayes, R.; Warr, G. G.; Atkin, R. Structure and Nanostructure in Ionic Liquids. *Chem. Rev.* **2015**, *115*, 6357−6426.

(3) Araque, J. C.; Hettige, J. J.; Margulis, C. J. Modern Room Temperature Ionic Liquids, a Simple Guide to Understanding Their Structure and How It May Relate to Dynamics. *J. Phys. Chem. B* **2015**, *119*, 12727−12740.

(4) Hallett, J. P.; Welton, T. Room-Temperature Ionic Liquids: Solvents for Synthesis and Catalysis. 2. *Chem. Rev.* **2011**, *111*, 3508−3576.

(5) Plechkova, N. V.; Seddon, K. R. Applications of Ionic Liquids in the Chemical Industry. *Chem. Soc. Rev.* **2008**, *37*, 123−150.

(6) Welton, T. Room-Temperature Ionic Liquids. Solvents for Synthesis and Catalysis. *Chem. Rev.* **1999**, *99*, 2071−2084.

(7) Armand, M.; Endres, F.; MacFarlane, D. R.; Ohno, H.; Scrosati, B. Ionic-Liquid Materials for the Electrochemical Challenges of the Future. *Nat. Mater.* **2009**, *8*, 621−629.

(8) Shirota, H.; Mandai, T.; Fukazawa, H.; Kato, T. Comparison between Dicationic and Monocationic Ionic Liquids: Liquid Density, Thermal Properties, Surface Tension, and Shear Viscosity. *J. Chem. Eng. Data* **2011**, *56*, 2453−2459.

(9) Souda, R. Glass−Liquid Transition, Crystallization, and Melting of a Room Temperature Ionic Liquid: Thin Films of 1-Ethyl-3-Methylimidazolium Bis[Trifluoromethanesulfonyl]Imide Studied with Tof-Sims. *J. Phys. Chem. B* **2008**, *112*, 15349−15354.

(10) Suarez, S. N.; Rúa, A.; Cuffari, D.; Pilar, K.; Hatcher, J. L.; Ramati, S.; Wishart, J. F. Do TFSA Anions Slither? Pressure Exposes the Role of TFSA Conformational Exchange in Self-Diffusion. *J. Phys. Chem. B* **2015**, *119*, 14756−14765.

(11) MacFarlane, D. R.; Forsyth, M.; Howlett, P. C.; Pringle, J. M.; Sun, J.; Annat, G.; Neil, W.; Izgorodina, E. I. Ionic Liquids in Electrochemical Devices and Processes: Managing Interfacial Electrochemistry. *Acc. Chem. Res.* **2007**, *40*, 1165−1173.

(12) Lewandowski, A.; Świderska-Mocek, A. Ionic Liquids as Electrolytes for Li-Ion Batteries—an Overview of Electrochemical Studies. *J. Power Sources* **2009**, *194*, 601−609.

(13) Galiński, M.; Lewandowski, A.; Stępniak, I. Ionic Liquids as Electrolytes. *Electrochim. Acta* **2006**, *51*, 5567−5580.

(14) Hagiwara, R.; Lee, J. S. Ionic Liquids for Electrochemical Devices. *Electrochemistry* **2007**, *75*, 23−34.

(15) MacFarlane, D. R.; Tachikawa, N.; Forsyth, M.; Pringle, J. M.; Howlett, P. C.; Elliott, G. D.; Davis, J. H.; Watanabe, M.; Simon, P.; Angell, C. A. Energy Applications of Ionic Liquids. *Energy Environ. Sci.* **2014**, *7*, 232−250.

(16) Shannon, M. S.; Bara, J. E. Properties of Alkylimidazoles as Solvents for CO_2 Capture and Comparisons to Imidazolium-Based Ionic Liquids. *Ind. Eng. Chem. Res.* **2011**, *50*, 8665−8677.

(17) Torralba-Calleja, E.; Skinner, J.; Gutierrez-Tauste, D. CO_2 Capture in Ionic Liquids: A Review of Solubilities and Experimental Methods. *J. Chem.* **2013**, *2013*, 1.

(18) Condemarin, R.; Scovazzo, P. Gas Permeabilities, Solubilities, Diffusivities, and Diffusivity Correlations for Ammonium-Based Room Temperature Ionic Liquids with Comparison to Imidazolium and Phosphonium RTIL Data. *Chem. Eng. J.* **2009**, *147*, 51−57.

(19) Giammanco, C. H.; Kramer, P. L.; Fayer, M. D. Dynamics of Dihydrogen Bonding in Aqueous Solutions of Sodium Borohydride. *J. Phys. Chem. B* **2015**, *119*, 3546−3559.

(20) Giammanco, C. H.; Wong, D. B.; Fayer, M. D. Water Dynamics in Divalent and Monovalent Concentrated Salt Solutions. *J. Phys. Chem. B* **2012**, *116*, 13781−13792.

(21) Kropman, M. F.; Bakker, H. J. Dynamics of Water Molecules in Aqueous Solvation Shells. *Science* **2001**, *291*, 2118−2120.

(22) Kropman, M. F.; Bakker, H. J. Vibrational Relaxation of Liquid Water in Ionic Solvation Shells. *Chem. Phys. Lett.* **2003**, *370*, 741−746.

(23) Omta, A. W.; Kropman, M. F.; Woutersen, S.; Bakker, H. J. Influence of Ions on the Hydrogen-Bond Structure in Liquid Water. *J. Chem. Phys.* **2003**, *119*, 12457−12461.

(24) Smith, J. D.; Saykally, R. J.; Geissler, P. L. The Effect of Dissolved Halide Anions on Hydrogen Bonding in Liquid Water. *J. Am. Chem. Soc.* **2007**, *129*, 13847−13856.

(25) Guàrdia, E.; Marti, J.; Garcia-Tarres, L.; Laria, D. A Molecular Dynamics Simulation Study of Hydrogen Bonding in Aqueous Ionic Solutions. *J. Mol. Liq.* **2005**, *117*, 63−67.

(26) Akitt, J. W. Multinuclear Nuclear Magnetic-Resonance Studies of Aqueous-Solutions of Tetrafluoroborate Salts. *J. Chem. Soc., Faraday Trans. 1* **1975**, *71*, 1557−1572.

(27) Moilanen, D. E.; Wong, D.; Rosenfeld, D. E.; Fenn, E. E.; Fayer, M. D. Ion-Water Hydrogen-Bond Switching Observed with 2D IR Vibrational Echo Chemical Exchange Spectroscopy. *Proc. Natl. Acad. Sci. U.S.A.* **2009**, *106*, 375−380.

(28) Park, S.; Moilanen, D. E.; Fayer, M. D. Water Dynamics-the Effects of Ions and Nanoconfinement. *J. Phys. Chem. B* **2008**, *112*, 5279−5290.

(29) Park, S.; Fayer, M. D. Hydrogen Bond Dynamics in Aqueous Nabr Solutions. *Proc. Natl. Acad. Sci. U.S.A.* **2007**, *104*, 16731−16738.

(30) Brink, G.; Falk, M. Infrared Spectrum of HDO in Aqueous Solutions of Perchlorates and Tetrafluoroborates. *Can. J. Chem.* **1970**, *48*, 3019−3025.

(31) Ji, M.; Odelius, M.; Gaffney, K. J. Large Angular Jump Mechanism Observed for Hydrogen Bond Exchange in Aqueous Perchlorate Solution. *Science* **2010**, *328*, 1003−1005.

(32) Marcus, Y. Effect of Ions on the Structure of Water: Structure Making and Breaking. *Chem. Rev.* **2009**, *109*, 1346−1370.

(33) Wong, D. B.; Giammanco, C. H.; Fenn, E. E.; Fayer, M. D. Dynamics of Isolated Water Molecules in a Sea of Ions in a Room Temperature Ionic Liquid. *J. Phys. Chem. B* **2013**, *117*, 623−635.

(34) Kramer, P. L.; Giammanco, C. H.; Fayer, M. D. Dynamics of Water, Methanol, and Ethanol in a Room Temperature Ionic Liquid. *J. Chem. Phys.* **2015**, *142*, No. 212408.

(35) Fadeeva, T. A.; Husson, P.; DeVine, J. A.; Costa Gomes, M. F.; Greenbaum, S. G.; Castner, E. W. Interactions between Water and 1-Butyl-1-Methylpyrrolidinium Ionic Liquids. *J. Chem. Phys.* **2015**, *143*, No. 064503.

DOI: 10.1021/acs.jpcb.6b07145
J. Phys. Chem. B 2016, 120, 9997−10009

(36) Hou, J.; Zhang, Z.; Madsen, L. A. Cation/Anion Associations in Ionic Liquids Modulated by Hydration and Ionic Medium. *J. Phys. Chem. B* **2011**, *115*, 4576−4582.
(37) Araque, J. C.; Yadav, S. K.; Shadeck, M.; Maroncelli, M.; Margulis, C. J. How Is Diffusion of Neutral and Charged Tracers Related to the Structure and Dynamics of a Room-Temperature Ionic Liquid? Large Deviations from Stokes−Einstein Behavior Explained. *J. Phys. Chem. B* **2015**, *119*, 7015−7029.
(38) Araque, J. C.; Daly, R. P.; Margulis, C. J. A Link between Structure, Diffusion and Rotations of Hydrogen Bonding Tracers in Ionic Liquids. *J. Chem. Phys.* **2016**, *144*, No. 204504.
(39) Kaintz, A.; Baker, G.; Benesi, A.; Maroncelli, M. Solute Diffusion in Ionic Liquids, NMR Measurements and Comparisons to Conventional Solvents. *J. Phys. Chem. B* **2013**, *117*, 11697−11708.
(40) Canongia Lopes, J. N.; Costa Gomes, M. F.; Pádua, A. A. H. Nonpolar, Polar, and Associating Solutes in Ionic Liquids. *J. Phys. Chem. B* **2006**, *110*, 16816−16818.
(41) Köddermann, T.; Paschek, D.; Ludwig, R. Molecular Dynamic Simulations of Ionic Liquids: A Reliable Description of Structure, Thermodynamics and Dynamics. *ChemPhysChem* **2007**, *8*, 2464−2470.
(42) Moreno, M.; Castiglione, F.; Mele, A.; Pasqui, C.; Raos, G. Interaction of Water with the Model Ionic Liquid [Bmim][BF4]: Molecular Dynamics Simulations and Comparison with NMR Data. *J. Phys. Chem. B* **2008**, *112*, 7826−7836.
(43) Fumino, K.; Wulf, A.; Ludwig, R. Strong, Localized, and Directional Hydrogen Bonds Fluidize Ionic Liquids. *Angew. Chem., Int. Ed.* **2008**, *47*, 8731−8734.
(44) Suo, L.; Borodin, O.; Gao, T.; Olguin, M.; Ho, J.; Fan, X.; Luo, C.; Wang, C.; Xu, K. "Water-in-Salt" Electrolyte Enables High-Voltage Aqueous Lithium-Ion Chemistries. *Science* **2015**, *350*, 938−943.
(45) Shimizu, K.; Freitas, A. A.; Atkin, R.; Warr, G. G.; FitzGerald, P. A.; Doi, H.; Saito, S.; Ueno, K.; Umebayashi, Y.; Watanabe, M.; Canongia Lopes, J. N. Structural and Aggregate Analyses of (Li Salt + Glyme) Mixtures: The Complex Nature of Solvate Ionic Liquids. *Phys. Chem. Chem. Phys.* **2015**, *17*, 22321−22335.
(46) Tachikawa, N.; Yamauchi, K.; Takashima, E.; Park, J.-W.; Dokko, K.; Watanabe, M. Reversibility of Electrochemical Reactions of Sulfur Supported on Inverse Opal Carbon in Glyme-Li Salt Molten Complex Electrolytes. *Chem. Commun.* **2011**, *47*, 8157−8159.
(47) Lawler, C.; Fayer, M. D. The Influence of Lithium Cations on Dynamics and Structure of Room Temperature Ionic Liquids. *J. Phys. Chem. B* **2013**, *117*, 9768−9774.
(48) Borodin, O.; Smith, G. D.; Henderson, W. Li + Cation Environment, Transport, and Mechanical Properties of the LiTFSI Doped N-Methyl-N-Alkylpyrrolidinium + TFSI- Ionic Liquids. *J. Phys. Chem. B* **2006**, *110*, 16879−16886.
(49) Umebayashi, Y.; Hamano, H.; Seki, S.; Minofar, B.; Fujii, K.; Hayamizu, K.; Tsuzuki, S.; Kameda, Y.; Kohara, S.; Watanabe, M. Liquid Structure of and Li + Ion Solvation in Bis-(Trifluoromethanesulfonyl)Amide Based Ionic Liquids Composed of 1-Ethyl-3-Methylimidazolium and N-Methyl-N-Propylpyrrolidinium Cations. *J. Phys. Chem. B* **2011**, *115*, 12179−12191.
(50) Monteiro, M. J.; Bazito, F. F. C.; Siqueira, L. J. A.; Ribeiro, M. C. C.; Torresi, R. M. Transport Coefficients, Raman Spectroscopy, and Computer Simulation of Lithium Salt Solutions in an Ionic Liquid. *J. Phys. Chem. B* **2008**, *112*, 2102−2109.
(51) Duluard, S.; Grondin, J.; Bruneel, J.-L.; Pianet, I.; Grélard, A.; Campet, G.; Delville, M.-H.; Lassègues, J.-C. Lithium Solvation and Diffusion in the 1-Butyl-3-Methylimidazolium Bis-(Trifluoromethanesulfonyl)Imide Ionic Liquid. *J. Raman Spectrosc.* **2008**, *39*, 627−632.
(52) Nicolau, B. G.; Sturlaugson, A.; Fruchey, K.; Ribeiro, M. C. C.; Fayer, M. D. Room Temperature Ionic Liquid-Lithium Salt Mixtures: Optical Kerr Effect Dynamical Measurements. *J. Phys. Chem. B* **2010**, *114*, 8350−8356.
(53) Mähler, J.; Persson, I. A Study of the Hydration of the Alkali Metal Ions in Aqueous Solution. *Inorg. Chem.* **2012**, *51*, 425−438.
(54) Bruni, F.; Imberti, S.; Mancinelli, R.; Ricci, M. A. Aqueous Solutions of Divalent Chlorides: Ions Hydration Shell and Water Structure. *J. Chem. Phys.* **2012**, *136*, No. 064520.
(55) Bakker, H. J. Structural Dynamics of Aqueous Salt Solutions. *Chem. Rev.* **2008**, *108*, 1456−1473.
(56) Stangret, J.; Gampe, T. Ionic Hydration Behavior Derived from Infrared Spectra in HDO. *J. Phys. Chem. A* **2002**, *106*, 5393.
(57) Bergström, P.-A.; Lindgren, J.; Kristiansson, O. An IR Study of the Hydration of ClO_4^-, NO_3^-, I^-, Br^-, Cl^-, and SO_4^{2-} Anions in Aqueous Solution. *J. Phys. Chem.* **1991**, *95*, 8575−8580.
(58) Adams, D. M.; Blandamer, M. J.; Symons, M. C. R.; Waddington, D. Solvation Spectra. Part 39.—Infra-Red and Raman Studies of Aqueous and Non-Aqueous Solutions Containing Perchlorates. *Trans. Faraday Soc.* **1971**, *67*, 611.
(59) Park, S.; Kwak, K.; Fayer, M. D. Ultrafast 2D-IR Vibrational Echo Spectroscopy: A Probe of Molecular Dynamics. *Laser Phys. Lett.* **2007**, *4*, 704−718.
(60) Fenn, E. E.; Wong, D. B.; Fayer, M. D. Water Dynamics in Small Reverse Micelles in Two Solvents: Two-Dimensional Infrared Vibrational Echoes with Two-Dimensional Background Subtraction. *J. Chem. Phys.* **2011**, *134*, No. 054512.
(61) Lawrence, C. P.; Skinner, J. L. Vibrational Spectroscopy of HOD in Liquid D_2O. II. Infrared Line Shapes and Vibrational Stokes Shift. *J. Chem. Phys.* **2002**, *117*, 8847−8854.
(62) Rey, R.; Møller, K. B.; Hynes, J. T. Hydrogen Bond Dynamics in Water and Ultrafast Infrared Spectroscopy. *J. Phys. Chem. A* **2002**, *106*, 11993−11996.
(63) Cammarata, L.; Kazarian, S. G.; Salter, P. A.; Welton, T. Molecular States of Water in Room Temperature Ionic Liquids. *Phys. Chem. Chem. Phys.* **2001**, *3*, 5192−5200.
(64) Fayer, M. D.; Moilanen, D. E.; Wong, D.; Rosenfeld, D. E.; Fenn, E. E.; Park, S. Water Dynamics in Salt Solutions Studied with Ultrafast Two-Dimensional Infrared (2D IR) Vibrational Echo Spectroscopy. *Acc. Chem. Res.* **2009**, *42*, 1210−1219.
(65) Kenkre, V. M.; Tokmakoff, A.; Fayer, M. D. Theory of Vibrational Relaxation of Polyatomic Molecules in Liquids. *J. Chem. Phys.* **1994**, *101*, 10618.
(66) Steinel, T.; Asbury, J. B.; Zheng, J. R.; Fayer, M. D. Watching Hydrogen Bonds Break: A Transient Absorption Study of Water. *J. Phys. Chem. A* **2004**, *108*, 10957−10964.
(67) Rezus, Y. L. A.; Bakker, H. J. On the Orientational Relaxation of HDO in Liquid Water. *J. Chem. Phys.* **2005**, *123*, No. 114502.
(68) Schmidt, J. R.; Corcelli, S. A.; Skinner, J. L. Pronounced Non-Condon Effects in the Ultrafast Infrared Spectroscopy of Water. *J. Chem. Phys.* **2005**, *123*, No. 044513.
(69) Pimentel, G. C.; McClellan, A. L. *The Hydrogen Bond*; W.H. Freeman and Co.: San Francisco, 1960.
(70) Moilanen, D. E.; Fenn, E. E.; Lin, Y. S.; Skinner, J. L.; Bagchi, B.; Fayer, M. D. Water Inertial Reorientation: Hydrogen Bond Strength and the Angular Potential. *Proc. Natl. Acad. Sci. U.S.A.* **2008**, *105*, 5295−5300.
(71) Moilanen, D. E.; Fenn, E. E.; Wong, D.; Fayer, M. D. Water Dynamics in Large and Small Reverse Micelles: From Two Ensembles to Collective Behavior. *J. Chem. Phys.* **2009**, *131*, No. 014704.
(72) Laage, D.; Hynes, J. T. A Molecular Jump Mechanism of Water Reorientation. *Science* **2006**, *311*, 832−835.
(73) Lipari, G.; Szabo, A. Effect of Librational Motion on Fluorescence Depolarization and Nuclear Magnetic-Resonance Relaxation in Macromolecules and Membranes. *Biophys. J.* **1980**, *30*, 489−506.
(74) Tan, H.-S.; Piletic, I. R.; Fayer, M. D. Orientational Dynamics of Water Confined on a Nanometer Length Scale in Reverse Micelles. *J. Chem. Phys.* **2005**, *122*, No. 174501.
(75) Kinosita, K.; Ikegami, A.; Kawato, S. On the Wobbling-in-Cone Analysis of Fluorescence Anisotropy Decay. *Biophys. J.* **1982**, *37*, 461−464.
(76) Giammanco, C. H.; Yamada, S. A.; Kramer, P. L.; Tamimi, A.; Fayer, M. D. Structural and Rotational Dynamics of Carbon Dioxide in

DOI: 10.1021/acs.jpcb.6b07145
J. Phys. Chem. B 2016, 120, 9997−10009

1-Alkyl-3-Methylimidazolium Bis(Trifluoromethylsulfonyl)Imide Ionic Liquids: The Effect of Chain Length. *J. Phys. Chem. B* **2016**, *120*, 6698.
(77) Tamimi, A.; Fayer, M. D. Ionic Liquid Dynamics Measured with 2D IR and IR Pump−Probe Experiments on a Linear Anion and the Influence of Potassium Cations. *J. Phys. Chem. B* **2016**, *120*, 5842.
(78) Stirnemann, G.; Laage, D. Direct Evidence of Angular Jumps During Water Reorientation through Two-Dimensional Infrared Anisotropy. *J. Phys. Chem. Lett.* **2010**, *1*, 1511−1516.
(79) Sturlaugson, A. L.; Arima, A. Y.; Bailey, H. E.; Fayer, M. D. Orientational Dynamics in a Lyotropic Room Temperature Ionic Liquid. *J. Phys. Chem. B* **2013**, *117*, 14775−14784.
(80) Kwak, K.; Rosenfeld, D. E.; Fayer, M. D. Taking Apart the Two-Dimensional Infrared Vibrational Echo Spectra: More Information and Elimination of Distortions. *J. Chem. Phys.* **2008**, *128*, No. 204505.
(81) Kwak, K.; Park, S.; Finkelstein, I. J.; Fayer, M. D. Frequency-Frequency Correlation Functions and Apodization in 2D-IR Vibrational Echo Spectroscopy, a New Approach. *J. Chem. Phys.* **2007**, *127*, No. 124503.
(82) Asbury, J. B.; Steinel, T.; Stromberg, C.; Corcelli, S. A.; Lawrence, C. P.; Skinner, J. L.; Fayer, M. D. Water Dynamics: Vibrational Echo Correlation Spectroscopy and Comparison to Molecular Dynamics Simulations. *J. Phys. Chem. A* **2004**, *108*, 1107−1119.
(83) Bakker, H. J.; Kropman, M. F.; Omta, Y.; Woutersen, S. Hydrogen-Bond Dynamics of Water in Ionic Solutions. *Phys. Scr.* **2004**, *69*, C14−C24.
(84) Laage, D.; Hynes, J. T. On the Residence Time for Water in a Solute Hydration Shell: Application to Aqueous Halide Solutions. *J. Phys. Chem. B* **2008**, *112*, 7697−7701.
(85) Giammanco, C. H.; Kramer, P. L.; Yamada, S. A.; Nishida, J.; Tamimi, A.; Fayer, M. D. Carbon Dioxide in an Ionic Liquid: Structural and Rotational Dynamics. *J. Chem. Phys.* **2016**, *144*, No. 104506.
(86) Kramer, P. L.; Nishida, J.; Fayer, M. D. Separation of Experimental 2D IR Frequency-Frequency Correlation Functions into Structural and Reorientation-Induced Contributions. *J. Chem. Phys.* **2015**, *143*, No. 124505.
(87) Kramer, P. L.; Nishida, J.; Giammanco, C. H.; Tamimi, A.; Fayer, M. D. Observation and Theory of Reorientation-Induced Spectral Diffusion in Polarization-Selective 2D IR Spectroscopy. *J. Chem. Phys.* **2015**, *142*, No. 184505.
(88) Novak, A. Hydrogen Bonding in Solids. In *Structure and Bonding*; Dunitz, J. D., Ed.; Springer-Verlag: Berlin, 1974; Vol. *18*; pp 177−216.
(89) Corcelli, S.; Lawrence, C. P.; Skinner, J. L. Combined Electronic Structure/Molecular Dynamics Approach for Ultrafast Infrared Spectroscopy of Dilute HOD in Liquid H_2O and D_2O. *J. Chem. Phys.* **2004**, *120*, 8107−8117.

DOI: 10.1021/acs.jpcb.6b07145
J. Phys. Chem. B 2016, 120, 9997−10009